Ultradian calcium rhythms in the paraventricular nucleus and subparaventricular zone in the hypothalamus

Yu-Er Wu[a,b,c,d,1], Ryosuke Enoki[d,e,1,2,3], Yoshiaki Oda[d,4], Zhi-Li Huang[a,b,c,2], Ken-ichi Honma[d], and Sato Honma[d]

[a]State Key Laboratory of Medical Neurobiology, School of Basic Medical Sciences, Fudan University, Shanghai 200032, China; [b]Institutes of Brain Science and Collaborative Innovation Center for Brain Science, Fudan University, Shanghai 200032, China; [c]Department of Pharmacology, School of Basic Medical Sciences, Fudan University, Shanghai 200032, China; [d]Research and Education Center for Brain Science, Hokkaido University Graduate School of Medicine, Sapporo 060-8638, Japan; and [e]Photonic Bioimaging Section, Research Center for Cooperative Projects, Hokkaido University Graduate School of Medicine, Sapporo 060-8638, Japan

The suprachiasmatic nucleus (SCN), the master circadian clock in mammals, sends major output signals to the subparaventricular zone (SPZ) and further to the paraventricular nucleus (PVN), the neural mechanism of which is largely unknown. In this study, the intracellular calcium levels were measured continuously in cultured hypothalamic slices containing the PVN, SPZ, and SCN. We detected ultradian calcium rhythms in both the SPZ-PVN and SCN regions with periods of 0.5–4.0 hours, the frequency of which depended on the local circadian rhythm in the SPZ-PVN region. The ultradian rhythms were synchronous in the entire SPZ-PVN region and a part of the SCN. Because the ultradian rhythms were not detected in the SCN-only slice, the origin of ultradian rhythm is the SPZ-PVN region. In association with an ultradian bout, a rapid increase of intracellular calcium in a millisecond order was detected, the frequency of which determined the amplitude of an ultradian bout. The synchronous ultradian rhythms were desynchronized and depressed by a sodium channel blocker tetrodotoxin, suggesting that a tetrodotoxin-sensitive network is involved in synchrony of the ultradian bouts. In contrast, the ultradian rhythm is abolished by glutamate receptor blockers, indicating the critical role of glutamatergic mechanism in ultradian rhythm generation, while a GABA$_A$ receptor blocker increased the frequency of ultradian rhythm and modified the circadian rhythm in the SCN. A GABAergic network may refine the circadian output signals. The present study provides a clue to unraveling the loci and network mechanisms of the ultradian rhythm.

intracellular calcium | fluorescence imaging | neuronal network | ultradian rhythm | circadian rhythm

Circadian rhythm is a widespread phenomenon underlying various physiological and behavioral processes in mammals. In the past few decades, a considerable body of knowledge has accumulated regarding the molecular machinery that drives circadian rhythms, involving transcriptional–translational feedback loops composed of clock genes and their protein products (1). In addition, in vivo studies have revealed that various functions of mammalian physiology fluctuate in a range from one to several hours (ultradian), such as behavioral arousal, rapid eye movement (REM)–non-REM sleep cycles, hormone release, locomotion, body temperature, and gene expression (2–5). Circadian and ultradian rhythms are not a simple reflection of environmental changes because they persist in the constant environmental condition. However, despite the broad recognition of ultradian cycles and their functional importance (6), we know very little about the pacemaker loci and mechanisms of the ultradian rhythms.

The hypothalamic suprachiasmatic nucleus (SCN), the master circadian clock in mammals, controls circadian rhythms in physiology and behavior (7). Interestingly, the ultradian rhythms persist, and even become more robust after surgical (8, 9) or genetic lesion of the SCN (10, 11). These results indicate the presence of an ultradian oscillator independent of the SCN circadian pace-

maker. The ultradian rhythms are also observed in other hypothalamic areas, such as gonadotropin-releasing hormone (GnRH) release in the preoptic area in the hypothalamus (12). However, whether this region alone constitutes the ultradian oscillation or whether this pathway is an output of the ultradian rhythm generated somewhere else remains unsolved. A fundamental obstacle in elucidating ultradian mechanisms appears to be a difficulty in identification of ultradian rhythms in vitro, despite that the ultradian rhythms of neuronal firing in the SCN-subparaventricular zone (SPZ) (13) and of clock gene expression in the SCN (2) have been reported in freely behaving animals.

SCN neurons send the major output signals to the SPZ and further to the paraventricular nucleus (PVN) region in the hypothalamus (14, 15) via diffusible factors, such as arginine vasopressin (AVP) (16) and neuronal projections (17, 18). The PVN is composed of a group of neurons, including neurosecretory cells, and synthesizes various hormones, such as a corticotropin-releasing hormone, oxytocin, and vasopressin (14). These hormones show the circadian rhythms with different peak times in their production

Significance

Despite that the various functions in mammals fluctuate in the ultradian fashion, the origin and mechanism of the rhythm are largely unknown. In this study, we found synchronous ultradian calcium rhythms in the hypothalamic paraventricular nucleus (PVN), subparaventricular zone (SPZ), and suprachiasmatic nucleus (SCN). The ultradian rhythms were originated from the SPZ-PVN region and transmitted to the SCN. Neurochemical interventions revealed that the glutamatergic mechanism is critical for generation and a tetrodotoxin-sensitive neural network for synchrony of the ultradian rhythm. The GABAergic system could have a role in refining the circadian output signals. The study provides the first clue to understand the loci and mechanism of ultradian rhythm in the hypothalamus.

and secretion. The PVN possesses the local circadian oscillator, which is independent of the SCN (19). The SPZ is known as a hub region, which relays the circadian information from the SCN to other brain regions and ultimately controls the circadian rhythms of various physiological processes, such as sleep–wake cycles and locomotor activities (19).

In our prior studies, we established time-lapse calcium imaging in cultured SCN slices (20) and revealed the topological patterns of circadian calcium rhythms in the SCN network with the dorsal SCN phase-ahead of the ventral counterpart (21). In the present study, we extended this approach in cultured slices containing the SCN and SPZ-PVN and successfully identified ultradian calcium rhythms in the SPZ-PVN, which were transmitted to the SCN. The present study provides a clue to unraveling the loci and network mechanisms driving ultradian rhythmicity in mammals.

Results

Ultradian Calcium Rhythms in the PVN and SPZ. Using a recombinant adeno-associated virus (AAV) and the neuron-specific promoter human synapsin (hSyn), the highly-sensitive genetically encoded calcium probe, GCaMP6s (22), was transfected in cultured slices containing the SCN, PVN, and SPZ (SCN-SPZ-PVN slice) regions or those excluding the SCN (SPZ-PVN–only slice) prepared from newborn mice [postnatal days (P) 4–6] (*SI Appendix*, Fig. S1*A*). We monitored the spatiotemporal dynamics of intracellular calcium in these regions at 10-min sampling intervals for up to 8.5 d (*SI Appendix*, Fig. S1*B*).

Fig. 1 and Movie S1 show the representative example of calcium signals in the SCN-SPZ-PVN slices. We detected circadian calcium rhythms in the SCN regions, showing the characteristic topological pattern with an advanced-phase in the dorsal region
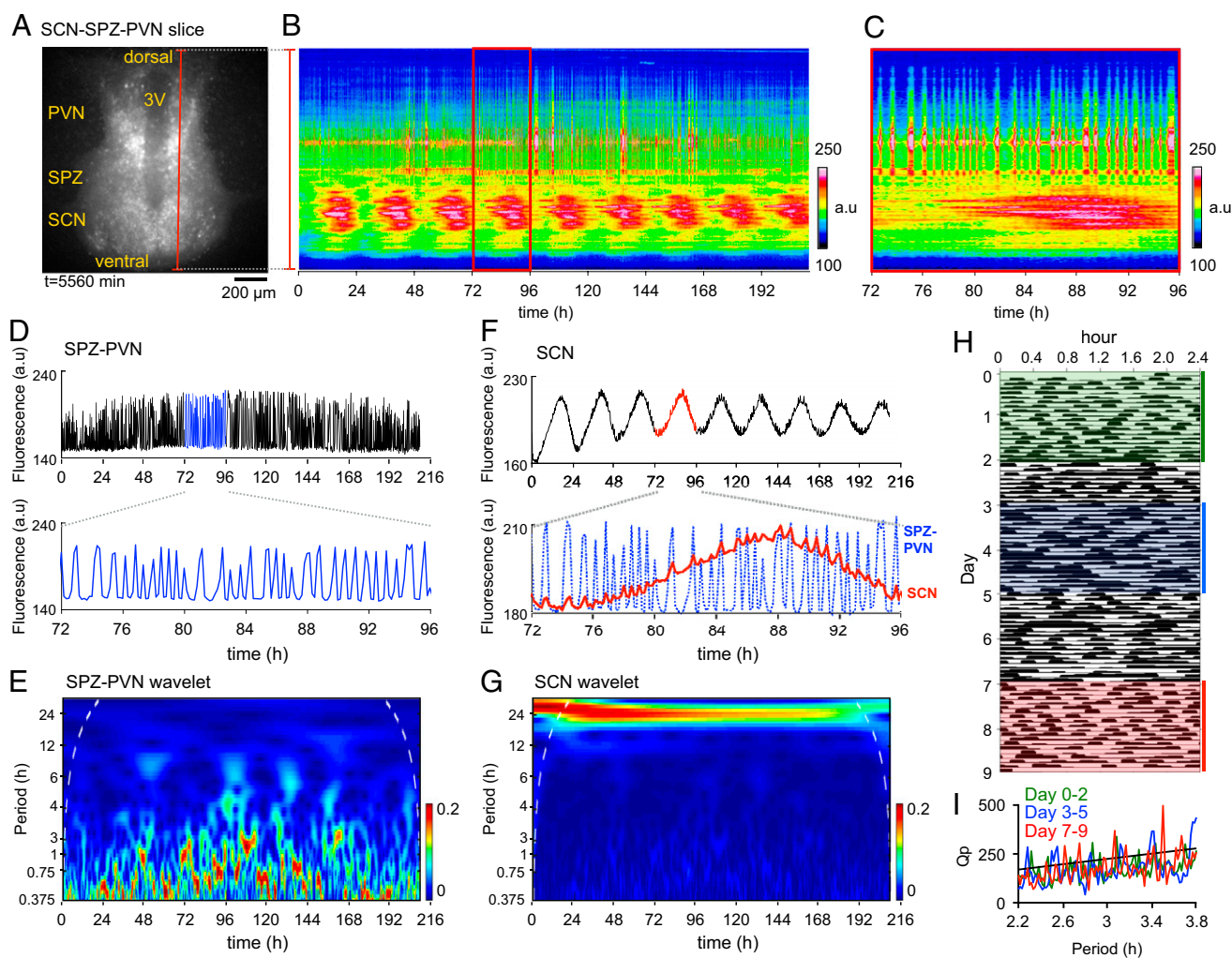

Fig. 1. Ultradian calcium rhythms in SCN-SPZ-PVN region. (*A*) Fluorescent images of the GCaMP6s signals in an SCN-SPZ-PVN slice. 3V, third ventricle. (*B*) Consecutive line scan image of the calcium rhythms for 216 h from the dorsal to the ventral region, as indicated by a red line in the slice images in *A*. A color bar in the right margin indicates the fluorescence intensity. (*C*) Expanded line-scan image for 24 h as indicated by a red rectangle area in *B*. Note that the ultradian calcium bouts are synchronous in the SPZ-PVN region up to the upper part of the SCN. (*D*) Time course of the ultradian calcium rhythm in the SPZ-PVN region during 216 h (over 8 d) of the recording (*Upper*) and a magnified view of the ultradian calcium rhythm in 72–96 h (*Lower*). (*E*) Wavelet spectrum of SPZ-PVN calcium rhythms in the rage of 0–30 h demonstrates ultradian calcium rhythms of 0.5- to 4.0-h periods. The magnitude of continuous wavelet transform coefficient is expressed as a heat map. The period in the y axis is expressed by the logarithmic scale. (*F*) Time course of the circadian calcium rhythms in the entire SCN region (*Upper*) and a magnified view of the circadian calcium rhythm in 72–96 h (*Lower*). SPZ-PVN ultradian bouts (blue dotted line) were superimposed with the SCN circadian rhythm (red solid line). Note that the timing of the ultradian bout on the circadian rhythm exactly coincides with that in the SPZ-PVN. (*G*) Wavelet spectrum of SCN calcium rhythms in the rage of 0–30 h demonstrates stable the circadian rhythms throughout the recording. (*H*) Ultradian calcium rhythms in the SPZ-PVN are expressed in a plotting along the x axis (2.4 h) and y axis (day). (*I*) A χ^2 periodogram is performed in a 2-d window as indicated by green, blue, and red areas in *H* and the results are expressed with the same colors. An oblique line in the periodogram indicates the significance level ($P < 0.01$). Note that the ultradian periodicity is changing during the recording.

compared with that in the center and ventral regions, as reported previously (Fig. 1 *B* and *C*) (20, 21, 23–25). By closer inspection, we found synchronous calcium signals with ultradian periods in the entire PVN and SPZ regions, which were extended up to the dorsal half of the SCN (Fig. 1 *B* and *C*). The synchronous ultradian rhythm actually consisted of a number of abrupt increases (bouts) of the intracellular calcium level (Fig. 1 *C* and *D*), which superimposed on the circadian fluctuation of the calcium signal in the SCN. Wavelet analysis (Fig. 1*E*) revealed the ultradian period ranging from 0.5 to 4.0 h in the SPZ-PVN region. The ultradian rhythms were unstable in periodicity, changing abruptly even within 24 h (Fig. 1*E*). Instability of the ultradian rhythms was confirmed by a plotting along the *x* axis (2.4 h) and *y* axis (day) (Fig. 1*H*). More than one ultradian rhythm is visible in this plot. Significant periodicities are detected by χ^2 periodogram ($P < 0.01$) (Fig. 1*I*). The major period changed depending on the culture days, confirming the results of wavelet analysis (Fig. 1*E*). We observed similar findings in other SCN-SPZ-PVN slices (*SI Appendix*, Figs. S2*D* and S3 *B* and *C*).

Local Circadian Rhythms in the SPZ-PVN Control the Frequency of Ultradian Bouts. Circadian fluctuations were visible in the calcium signals in the SPZ-PVN region of some but not all SCN-SPZ-PVN slices (Fig. 2*A* and *SI Appendix*, Fig. S2). The significance of circadian rhythm was evaluated by a cosine curve fitting method in the SCN and SPZ-PVN region separately. Seventeen of the 42 SCN-SPZ-PVN slices (40.5%) showed circadian rhythms in the SPZ-PVN regions (Fig. 2*B*), while all slices exhibited significant circadian rhythms in the SCN region. To examine the dependency of ultradian rhythm on the local circadian rhythm in the SPZ-PVN, the number and the amplitude of ultradian bouts were an-

alyzed in four circadian phases of the fitted cosine curves: the peak, falling, trough, and rising phases. The number of ultradian bouts was significantly larger at the rising phase compared with the trough phase ($n = 17$, $P = 0.031$, one-way ANOVA with a post hoc Tukey–Kramer test) (Fig. 2*C* and *SI Appendix*, Table S1). In contrast, such a phase-dependency was not detected in the amplitude of ultradian bouts (Fig. 2*D* and *SI Appendix*, Table S1). We measured the amplitudes of ultradian bouts in SPZ-PVN and SCN regions in individual slices and found that they are significantly correlated (788 bouts in 42 slices, $R^2 = 0.4541$, $P < 0.0001$, the amplitude was measured in a 24-h bin). The amplitude in the SPZ-PVN is 10 times larger than that in the SCN [54.2 ± 1.5 arbitrary units (a.u.) vs. 4.1 ± 0.2 a.u., mean $\pm$ SEM]. These results further support our conclusion that the origin of ultradian rhythm is the SPZ-PVN region.

There was no significant correlation in the circadian peak phase between the SPZ-PVN and SCN region ($R^2 = 0.087$, $P = 0.278$) (Fig. 2*E*). The period of circadian rhythms in the SCN and SPZ-PVN was not significantly different but the period in the SPZ-PVN was more variable (23.6 ± 0.19 h and 25.2 ± 0.94, respectively, $P = 0.122$). We analyzed the signal intensity of GCaMP6s at the baseline of oscillation with or without circadian rhythms in the SPZ-PVN regions to estimate whether or not the expression levels were identical between the two groups (187.3 ± 28.2 a.u. with circadian oscillation vs. 231.2 ± 29.2 a.u without circadian oscillation, mean $\pm$ SEM, $P = 0.24$, paired *t* test). We concluded that the reporter expression did not affect the circadian oscillation in the ultradian rhythms in the SPZ-PVN regions.

To further clarify the impact of the SCN circadian pacemaker on the local circadian rhythms in the SPZ-PVN, the SCN region was surgically removed and the SPZ-PVN–only slice was made. As seen
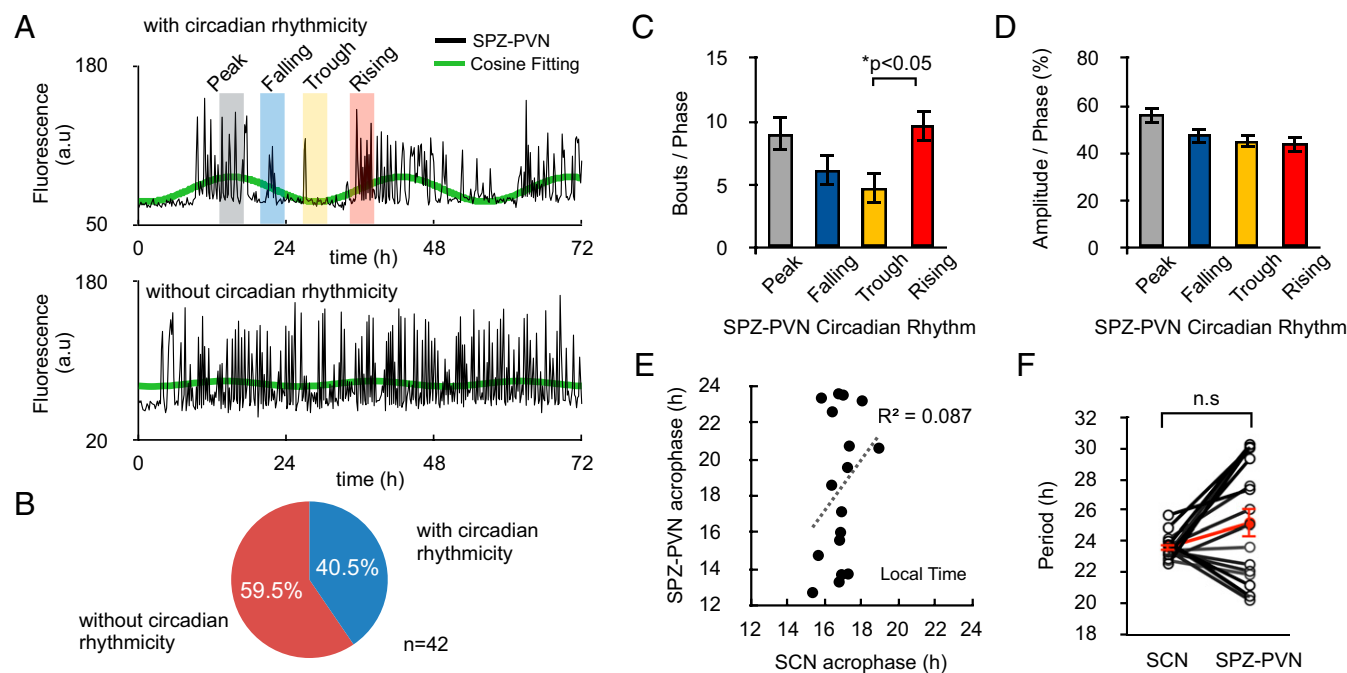

Fig. 2. Effects of circadian rhythmicity on ultradian rhythms in SPZ-PVN region. (*A*) Representative ultradian calcium rhythms with (*Upper*) and without (*Lower*) circadian rhythmicity in an SCN- SPZ-PVN slice. Green lines indicate the best-fitted cosine curves using 72-h consecutive calcium signals. The colored time windows (gray, blue, yellow, red) indicate four different circadian phases indicating the peak, falling, trough, and rising phase, respectively. (*B*) Percentage of the slices with/without circadian rhythmicity in the SPZ-PVN region; 40.5% of the slices have circadian rhythmicity in the SPZ-PVN region. (*C*) The mean number and its SEM of the ultradian bouts at four circadian phases. A calcium signal which exceeds the threshold of the normalized value was regarded as a bout (see details in *Materials and Methods*). The number at the rising phase was significantly larger than that at the trough ($n = 17$, $P = 0.031$, one-way ANOVA with a post hoc Tukey–Kramer test). (*D*) The mean amplitudes of the ultradian bouts at the four circadian phases. (*E*) A correlation between the acrophases of the circadian calcium rhythms in the SCN and SPZ-PVN region of the same slice. Acrophase is shown by local time. There is no significant correlation between SCN and SPZ-PVN acrophases ($R^2 = 0.087$, $P = 0.278$). (*F*) The period of circadian rhythms in the SCN and SPZ-PVN.

in *SI Appendix*, Figs. S4 and S5, none of the SPZ-PVN–only slices exhibited circadian fluctuation in their calcium signals, whereas the ultradian rhythms were still detectable (n = 21 slices). In the SCN-only slices, the circadian rhythms were preserved (*SI Appendix*, Fig. S6). Interestingly, the ultradian rhythms that superimposed on the circadian rhythm were abolished (*SI Appendix*, Fig. S6D). These results indicate that the ultradian rhythms are generated in the SPZ-PVN region and transmitted to the SCN.

TTX-Sensitive Neural Network, Glutamate, and GABA Signaling Are Involved in Ultradian Calcium Rhythms. It has been suggested that neurotransmitters, such as GABA, glutamate, and AVP are involved in the transmission of circadian signals from the SCN and in the neuronal interactions within the SPZ-PVN network (26–29). We tested the involvement of these systems in the SPZ-PVN ultradian and SCN circadian rhythms on the cellular as well as tissue level by blocking the neuronal transmission with specific receptor blockers in the SCN-SPZ-PVN slices.

Drug effects on the SPZ-PVN ultradian and SCN circadian rhythm on the tissue level. Application of the vehicle (DMEM) had no effect on the amplitude, bout number, or baseline level of the ultradian calcium rhythms in the whole SPZ-PVN region (Fig. 3A). A sodium channel blocker, tetrodotoxin (TTX; 1 μM), abolished the ultradian bouts and reduced the baseline level of the calcium signals (Fig. 3B). The amplitude of circadian calcium rhythm in the SCN region was moderately decreased, confirming our previous report (21). In addition, TTX smoothened the circadian fluctuation by eliminating the superimposed ultradian bouts (*SI Appendix*, Fig. S7B). After washout, the ultradian bouts gradually built up and the circadian amplitude recovered together with superimposed ultradian bouts. A mixture of AMPA- and NMDA-type glutamate receptor blockers (5 μM NBQX and 50 μM APV) completely suppressed the amplitude of ultradian bout and slightly the baseline of calcium signals (Fig. 3C). On the other hand, the circadian calcium rhythm in the SCN region was not affected significantly except for the elimination of superimposed ultradian bouts (*SI Appendix*, Fig. S7C). After washout, the ultradian bouts built up in the SPZ-PVN region and became superimposed on the circadian rhythm in the SCN region. In contrast, a mixture of AVP V1a and V1b receptor blockers (2.5 μM SR49059 and 2.5 μM SSR149415) had effects neither on the amplitude of ultradian bout in the SPZ-PVN region nor on the circadian calcium rhythm in the SCN region. In contrast, the GABA$_A$ receptor blocker gabazine (10 μM) seemed to decrease the amplitude and increase the baseline of calcium bout in the first 48 h and then build up the ultradian bouts of similar amplitude to that in pretreatment but with reversed downward direction. The amplitude of circadian rhythm in the SCN slightly was increased and the superimposed ultradian bouts became blurred in the first 48 h but reappear in a downward direction for the next 48 h (Fig. 3E). After washout, the baseline returned to the previous level and the reversed direction of the ultradian bouts was normalized. By closer inspection, the amplification of circadian rhythm is likely due to the elevation of ultradian baseline and blurredness of ultradian bouts is likely due to the small decrease in calcium signals (*SI Appendix*, Fig. S7E). We observed similar findings in other SCN-SPZ-PVN slices (*SI Appendix*, Fig. S8).

The drug effects on the number, amplitude, and baseline of the ultradian bouts in the SPZ-PVN region are summarized in *SI Appendix*, Fig. S9 and Table S1. TTX significantly decreased the number, amplitude, and baseline level of the ultradian bout compared with the pretreatment level (n = 6, P < 0.01, paired t test) (*SI Appendix*, Fig. S9B). NBQX and APV also significantly reduced all these parameters of the ultradian bout (*SI Appendix*, Fig. S9C) (n = 5, P < 0.01, paired t test). On the other hand, SR49059 and SSR149415 had no significant effect on these parameters (*SI Appendix*, Fig. S9D) (n = 5, n.s. paired t test). In contrast, gabazine affected these parameters in two steps (*SI*

Appendix, Fig. S9E). It apparently decreased the amplitude and increased the baseline of the ultradian bout for the first 48 h after application (n = 9, P < 0.001, paired t test). However, the amplitude gradually recovered in a reversed direction keeping a high baseline level for the following 48 h.

The drug effects on the circadian calcium rhythm in the SCN region of SCN-SPZ-PVN slice are summarized in *SI Appendix*, Fig. S10 and Table S1. The drug effects were examined on the acrophase SD as an index of network synchronization, the phase-difference between the dorsal and ventral regions, and the amplitude of circadian rhythm. TTX significantly desynchronized the SCN network, increased the phase-difference between the dorsal and ventral SCN, and decreased the amplitude (*SI Appendix*, Fig. S10B). On the other hand, gabazine had no effect either on the acrophase or on the phase difference. However, gabazine significantly increased the amplitude of circadian rhythm (*SI Appendix*, Fig. S10E).

These findings indicate the TTX-sensitive neural network, the glutamatergic, and GABAergic system in the SCN-SPZ-PVN are involved in the expression and transmission of the ultradian bouts. A loss of ultradian bouts superimposed on the circadian rhythm in the SCN region in association with the abolishment of ultradian rhythm in the SPZ-PVN region supports the idea that the ultradian rhythm is generated in the SPZ-PVN region and transferred to the SCN.

Drug effects on the SPZ-PVN ultradian rhythms and SCN circadian rhythm on the cellular level. We also examined the drug effects on the cellular level in the SCN-SPZ-PVN slice. We selected an isolated spot of cell size signal as a region-of-interest (ROI) and traced it for more than 12 d (288 h) (*SI Appendix*, Fig. S11). Synchronous ultradian bouts were confirmed in single cells of the SPZ-PVN region in the vehicle-treated slice (*SI Appendix*, Fig. S11A). TTX treatment reduced the amplitude of ultradian bout and desynchronized them. Interestingly, the baseline level of calcium signal increased and the ultradian bouts in some cells were reversed in downward direction. After washout, the amplitude recovered and synchrony was retained (*SI Appendix*, Fig. S11B). On the other hand, glutamate receptor blockers (5 μM NBQX and 50 μM APV) abolished the ultradian bout without changing the baseline level (*SI Appendix*, Fig. S11C). In contrast, a mixture of AVP V1a and V1b receptor blockers (2.5 μM SR49059 and 2.5 μM SSR149415) had no effects on these parameters of the ultradian bout, keeping synchrony among them (*SI Appendix*, Fig. S11D). Gabazine (10 μM) changed the ultradian bouts time-dependently. For the first 48 h, it seemed to increase the baseline and decrease the amplitude of ultradian bouts, and for the next 48 h it developed ultradian bouts with the downward direction (*SI Appendix*, Fig. S11E).

Fast and Synchronous Calcium Transients Underlie Ultradian Rhythms. To further investigate the mechanism of ultradian calcium bout in the SCN-SPZ-PVN slice, we increased time resolution by fast imaging at 30 fps for 20 s and repeated this acquisition session at 10-min intervals for 2 d.

We detected a rapid increase and gradual decrease of calcium signals (calcium transient) several times in 20 s (Fig. 4C). When the calcium transients were detected on the baseline, the amplitude of transient was large and the frequency of appearance was low. In contrast, when the transients were observed on the peak of the ultradian bout, the amplitude was low but the frequency was high (Fig. 4 B and C). When the calcium signals were scanned on a line from the dorsal to the ventral of SPZ-PVN region (Fig. 4D), they were expressed in a striped pattern with different intensities probably reflecting the cell level fluctuation. A larger magnification of timescale revealed calcium transients synchronous throughout the SPZ-PVN. The frequency of calcium transient is well coincident in time with the amplitudes of the ultradian bout (Fig. 4E). The relationship between the frequency and signal level is positively
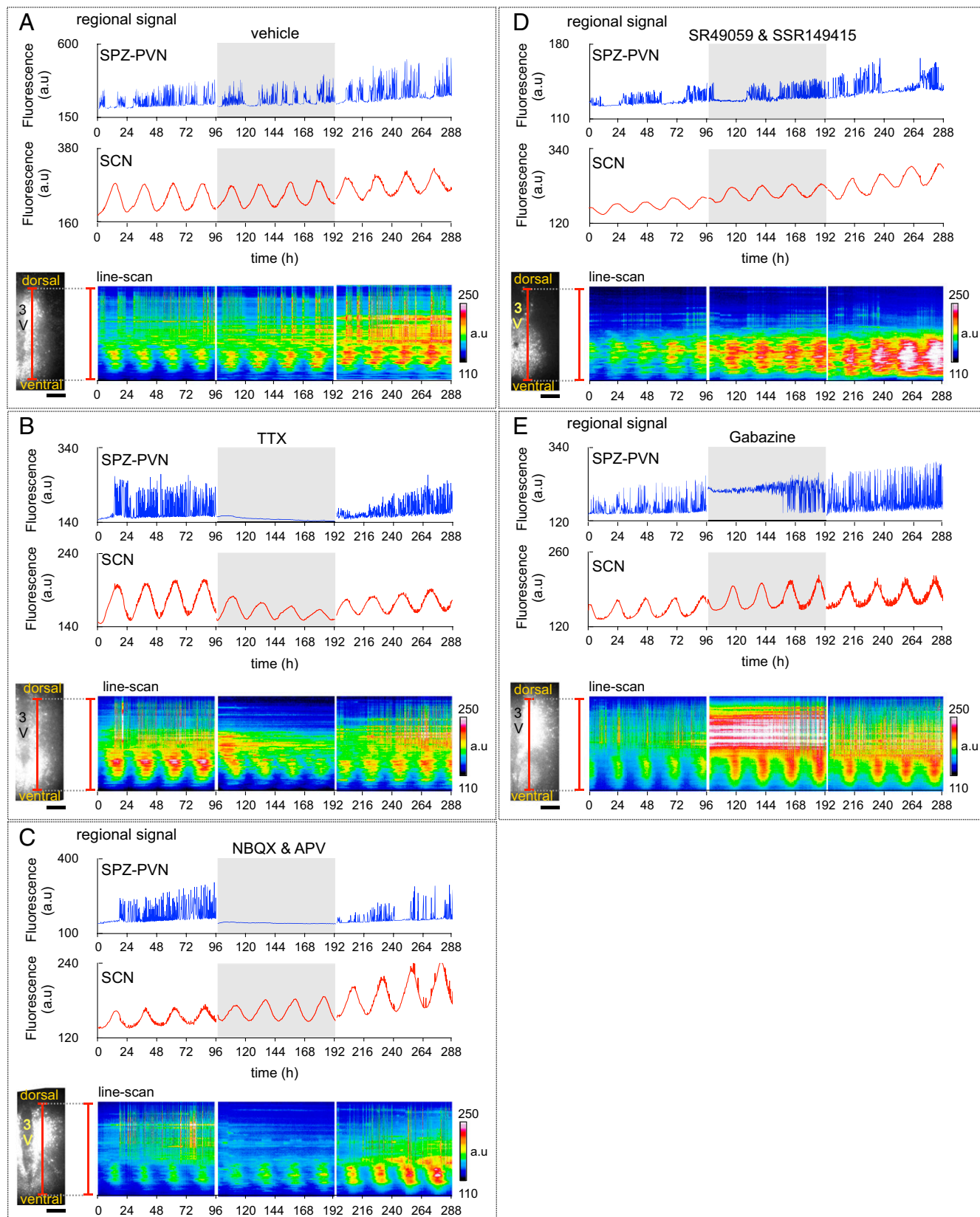
Fig. 3. Drug effects on the SPZ-PVN ultradian and SCN circadian calcium rhythms in the SCN-SPZ-PVN slices. (*A–E*) Time course of the ultradian calcium rhythm in SPZ-PVN region (*Upper*) and SCN circadian calcium rhythms in the SCN region (*Middle*) before, during (shadowed area), and after drug application. Drugs were applied for 96 h and then washed out by exchanging the culture medium. Line-scan image of calcium signals across the SCN and SPZ-PVN from the dorsal to the ventral region as indicated by a red line in slice images (*Lower*). (*A*) Vehicle (DMEM), (*B*) TTX (1 μM), (*C*) NBQX (5 μM) and APV (50 μM), (*D*) SR49059 (2.5 μM) and SSR149415 (2.5 μM), and (*E*) gabazine (10 μM) on the SPZ-PVN ultradian and SCN circadian calcium rhythm. (Scale bar: 100 μm.)
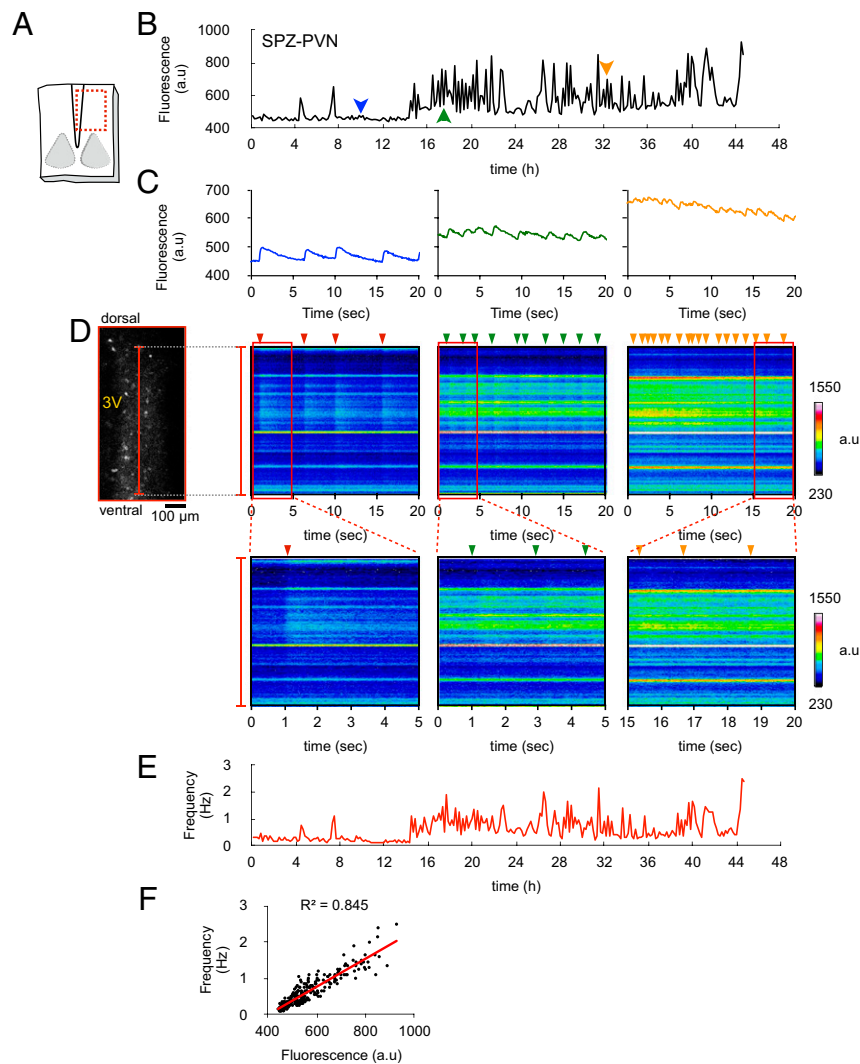
Fig. 4. Fast calcium imaging in the SPZ-PVN region. (*A*) Schematic drawing of an SCN-SPZ-PVN slice. A red-colored square indicates the SPZ-PVN region. (*B*) Time course of the calcium signal at 0.1–1.0 fps in the SPZ-PVN region for 45 h. The signals were taken at 10-min intervals. (*C*) Fast calcium transients recorded at 30 fps for 20 s. Calcium transients are shown in three different time points as indicated by arrows of the same color in *B*. (*D, Left*) Image of calcium signals in the area enclosed by a red square in the slice in *A*. (*D, Upper Right*) Line-scan images of the calcium transients from the dorsal to the ventral region as indicated by a red line in *D*. Arrows on the top show the timing of the calcium transients. (*D, Lower Right*) Expanded line-scan images as indicated by red rectangular areas in *Upper* images. (*E*) Time course of the frequency (Hz) of ultradian calcium bouts. (*F*) A correlation of the intensity of calcium signal (*x* axis) and the frequency of calcium transients (*y* axis). A positive correlation ($R^2 = 0.845$) is shown by a linear regression line (red).

correlated ($R^2 = 0.845$) (Fig. 4*F*). We also measured the amplitude of ultradian bouts in SPZ-PVN and SCN regions in all recordings and found the positive correlation between two regions ($R^2 = 0.4541$, $P < 0.0001$).

We observed similar findings in other SPZ-SPZ-PVN slices (*SI Appendix*, Fig. S12). The frequency, amplitude, rise time, and one-half decay time of the calcium transients are 0.14 ± 0.05 Hz, $12.3 \pm 1.26\%$, 0.44 ± 0.02 s, and 1.63 ± 0.15 s, respectively, during the baseline (quiet) (120 traces, $n = 6$ slices) (*SI Appendix*, Fig. S13 and Table S1).

Drug Effects on Synchronous Calcium Transients in the SPZ-PVN Region. To understand the drug effects on the ultradian calcium bouts at the level of calcium transients, we performed the fast imaging for the SCN-SPZ-PVN slices treated with one of the above-mentioned drugs (Fig. 5). TTX (80 traces, $n = 4$ slices) substantially suppressed the ultradian bouts and calcium transients (Fig. 5*A* and *SI Appendix*, Fig. S13), but the calcium transients were still detectable in some cells. NBQX and APV (80 traces, $n = $

4 slices) completely suppressed the calcium transients (Fig. 5*B* and *SI Appendix*, Fig. S13). In contrast, AVP receptor blockers had no significant effect on the calcium transients (140 traces, $n = 7$ slices) (Fig. 5*C* and *SI Appendix*, Fig. S13). On the other hand, gabazine significantly increased the amplitude and lengthened the rise time of the calcium transients (80 traces, $n = 4$ slices) (Fig. 5*D* and *SI Appendix*, Fig. S13). It did not affect the synchrony of calcium transients. A positive correlation was preserved between the frequency and strength of calcium signals even in the presence of SR49059 and SSR149415 or gabazine (Fig. 5 *C, v* and *D, v*).

The drug effects on the frequency, amplitude, rise time and decay time of calcium transients are summarized in *SI Appendix*, Fig. S13 and Table S1. AVP receptor blockers had no effect on these parameters, while gabazine significantly increased the amplitude and rise time without affecting the decay time.

Discussion

In the present study, we found the ultradian rhythms in the range of 0.5–4.0 h in intracellular calcium level in the SPZ-PVN and
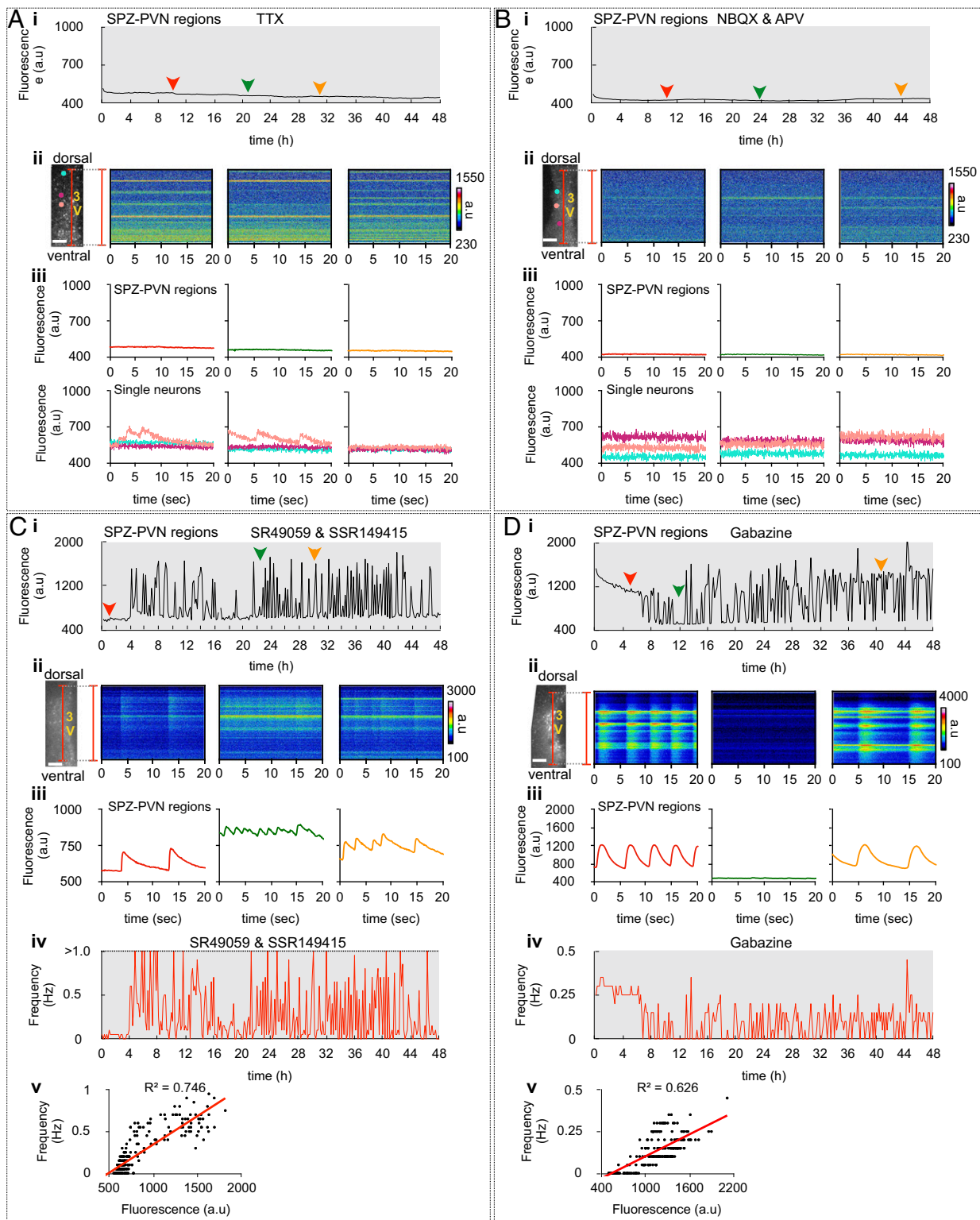
Fig. 5. Drug effects on fast calcium transients in the SPZ-PVN region of an SCN-SPZ-PVN slice. Effect of TTX (*A*), NBQX and APV (*B*), SR49059 and SSR149415 (*C*), and gabazine (*D*) on fast calcium transients in the SPZ-PVN region. (*i*) Time course of the calcium signals in time-lapse imaging of 0.1–1 fps for 48 h. (*ii*, *Left*) Image of calcium signals in SPZ-PVN region. (*ii*, *Right*) Line-scan images of 30 fps for 20 s from the dorsal to the ventral region as indicated by a red line in the *Left*. (*iii*, *Upper*) Fast calcium transients at SPV-PVN region recorded at different times indicated by different colored triangles in *i*. (*iii*, *Lower*) Three representative traces of single SPZ-PVN neurons. Cell body size ROIs were selected as indicated by colored dots in *ii*. (*iv*) Time course of the frequency (Hz) of ultradian bouts. (*v*) The relationship between the intensity of calcium signal (*x* axis) and frequency of calcium transients (*y* axis). A linear regression line is shown by a red line with a regression coefficient (R^2). See also the legend of Fig. 3.

NEUROSCIENCE

SCN regions of cultured slices from neonatal mice. The ultradian rhythms are synchronous in the entire area of the SPZ-PVN and a part of the SCN. A slice culture of the SCN alone does not exhibit the ultradian rhythm and chemical interruption of the neural network abolishes the ultradian rhythms in the SCN together with those in the SPZ-PVN, indicating that the origin of ultradian rhythm is the SPZ-PVN region. Each ultradian calcium bout is composed of a number of fast intracellular calcium increase (transient) in the millisecond order, the frequency of which determines the amplitude of an ultradian bout. These findings indicate the origin of ultradian rhythm in the SCN and the neurochemical mechanism of neural networks involved.

SPZ-PVN Is the Origin of Ultradian Calcium Rhythms. Ultradian rhythms of 0.5- to 4.0-h periods are detected in the intracellular calcium in the cultured SCN-SPZ-PVN slice (Fig. 1). They are synchronous in the entire area examined. Previously, the ultradian rhythms of neuronal firing in the SPZ (13) and clock gene expression (*Per2*) in the SCN (2) have been reported in freely behaving adult animals using multiunit neural activity recording and fiber-optic bioluminescence recording, respectively. However, the origin of ultradian rhythms in the SCN was not elucidated. In the present study, the ultradian calcium rhythms in the SCN are found to originate from the SPZ-PVN region. Because the SCN-only slice does not show the ultradian rhythms and because the SPZ-PVN–only slices still exhibit the ultradian rhythm, the origin of ultradian rhythm is safely concluded to be the SPZ-PVN region. The ultradian signals are transmitted from this region to the SCN and exhibit the ultradian rhythms in intracellular calcium levels. Because the intracellular calcium influences the neuronal activity and the core molecular loop of circadian rhythm generation, it is highly plausible that the ultradian rhythms in *Per2* expression are also originated in the SPZ-PVN region.

The frequency of ultradian calcium rhythm is not stable in the course of culture. This is partly because of involvement of more than one ultradian rhythm in the intracellular calcium (Fig. 1 *H* and *I* and *SI Appendix*, Fig. S3). The interaction of multiple ultradian rhythms may give rise to lability in the ultradian frequency. The frequency of ultradian rhythm depends to some extent on the phase of local circadian rhythm in the SPZ-PVN (Fig. 2 *C* and *D*). The frequency is highest in the rising phase of circadian rhythm and lowest in the trough. A similar clustering of ultradian bouts has been reported (2, 13), suggesting the physiological significance of the ultradian bouts in the neurosecretion from the SPZ-PVN. PVN neurohormones, such as a corticotropin-releasing hormone, oxytocin, and vasopressin, are known to be secreted in an ultradian fashion and at a different time of day, indicating that the time of secretion is regulated by the circadian rhythm (30, 31). The multiplicity of ultradian periods could reflect the different ultradian patterns of neurosecretion. In addition, many hormones are secreted in ultradian patterns, which are thought to be important for the maintenance of tissue responsiveness by avoiding receptor down-regulation (32). The PVN is also known as an important nucleus in feeding/drinking behaviors. These behaviors in mice exhibit ultradian rhythms, which are modified by the circadian rhythm (33, 34). Before the full development of circadian rhythmicity in rodents, the behaviors of pups especially exhibit the ultradian rhythms, most of which may reflect ultradian suckling (35). The ultradian calcium rhythm in the SPZ-PVN could be related with the ultradian sucking behavior of pup mice.

Circadian rhythmicity in intracellular calcium levels is detected in the SPZ-PVN region of the 40% of SCN-SPZ-PVN slices (Fig. 2). Interestingly, the circadian peak phases in the SCN and SPZ-PVN region were not correlated (Fig. 2*E*), suggesting that the local circadian rhythm in the SPZ-PVN region desynchronized from the SCN circadian rhythm. However, the acrophase of the SPZ-PVN circadian rhythm distributed over a limited range (approximately 12 h) of the phase of the SCN circadian rhythm, implying that they

were not completely independent. In this respect, a large variability of the period in the SPZ-PVN (Fig. 2*F*) suggested relative co-ordination of the SPZ-PVN circadian rhythm to the SCN rhythm (36). On the other hand, significant circadian calcium rhythm was not detected in any of the SPZ-PVN–only slices (*SI Appendix*, Fig. S6). Because the circadian rhythm in *Per1* expression has been reported in the cultured hypothalamic slice without the SCN (37), the disappearance of local circadian rhythm in this region was not due to the stop of circadian oscillation but most likely to the damping of overt circadian rhythms. Under desynchronization, the circadian rhythm is known to be strongly damped (38, 39).

Fast Calcium Transients Underlie Ultradian Rhythms. By using a fast calcium imaging at 30 fps, we successfully detected calcium transients in the order of milliseconds. Calcium transients consist of a phase of rapid increase in calcium signals and a phase of exponential decay of it. Importantly, the frequency of calcium transient correlates positively with the strength of calcium signals, namely the amplitude of ultradian bout (Fig. 4 and *SI Appendix*, Fig. S12). This correlation suggests that a single ultradian bout is composed of multiple calcium transients and the number of transients determines the amplitude of an ultradian bout. Because the decay time is longer by approximately three times than the rise time, the more frequently the calcium transient occurs, the higher the calcium signal or the baseline of calcium transient becomes. The calcium transients in the SPZ-PVN are synchronous throughout the region. It has been reported that oxytocin- and vasopressin-producing neurosecretory cells in the PVN display bursting activity of action potentials both in vivo and in vitro, which occurs synchronously throughout the population of the PVN (27–29). The intensity of calcium signals is strong in the middle of the PVN and rather weak in the SPZ, which are consistent with the location of neurosecretory cells. Calcium transients could reflect the bursting activity of these neurons in the PVN. It has been suggested that activity-dependent depletion in extracellular calcium (40) or change in the extracellular electric field (41) contribute to the information processing in the neuronal network. These "non-synaptic" mechanisms could be involved in synchronization of the neighboring neurons in the SPZ-PVN region.

Neurochemical Mechanisms of Ultradian Calcium Rhythms. The mechanism of ultradian oscillation is not well understood. It could be a molecular oscillation similar to the core loop for circadian rhythm generation. The best example has been proposed for the tissue morphogenesis and somitogenesis (42, 43). The ultradian rhythms of approximately 2-h periodicity in the segmentation of somites is coupled to the transcriptional negative feedback loop of Hes1/7 and to the Delta-like 1 (Dll1)-Notch signalings between the adjacent cells. A model combining of an autoregulatory molecular feedback and cell–cell interaction dynamics has been proposed (43). The other is an oscillatory circuit of the neuronal network, and the several models for the ultradian rhythm generation have been proposed in the preoptic area (12), intergeniculate leaflet (44), and SCN (45). In this respect, it is interesting to note that while TTX substantially decreases the amplitude of ultradian bout, there still remain the ultradian bouts on the cell level, which desynchronized each other (*SI Appendix*, Fig. S11B). Similarly, calcium transients are detected in some cells treated with TTX (Fig. 5 *A*, *iii*). These findings suggest that the ultradian oscillation is cell origin and the TTX-sensitive neural network is involved in synchronization of cellular ultradian oscillations, which amplifies the ultradian bout. On the other hand, the glutamatergic system could be directly involved in the generation of calcium transient and ultradian bout, by blocking an inward flow of calcium ions. The possibility is supported by the glutamatergic inputs within the PVN network, which play a key role in controlling bursting activity of neurons (32–34). Taken together, these data show that the

ultradian calcium rhythms in the SPZ-PVN region are likely synchronized rhythms of multiple cellular calcium oscillations.

On the other hand, the role of GABAergic network is quite different from TTX and glutamate receptor antagonists. Gabazine, a GABA$_A$ receptor antagonist, increases the baseline of the ultradian bout and reverses the direction of the bout to downward (Fig. 4E). The elevation of the baseline is likely due to a bulk of ultradian bouts occurring in high frequency, which masks the rising and falling phases of ultradian bouts resulting in the continuation of bout peaks. The continuation of bout peaks is more likely interpretation than the elevation of baseline. And a downward ultradian bout is also due to the continuation of high-frequency bouts and a transient pause of bouts, which apparently make the reversed shape of the bout. Gabazine increases the amplitude of circadian rhythm in the SCN regions and reverses the direction of superimposed ultradian bouts (*SI Appendix*, Fig. S7E). These effects are also ascribed to the high frequency of ultradian bouts and the continuation of bout peaks. The role of the GABAergic network in these regions is likely to exclude noisy ultradian signals and to refine the circadian signals in the SCN.

The ultradian components in the circadian calcium rhythm in the SCN region disappear after TTX or NBQX and APV treatment (*SI Appendix*, Fig. S7 B and C). This may simply be the result of suppression or abolishment of ultradian rhythms in the SPZ-PVN region.

Conclusions

Ultradian rhythms of 0.5- to 4.0-h period are detected in the intracellular calcium level in the SCN and SPZ-PVN regions of the SCN-SPZ-PVN culture slices from neonatal mice. The ultradian rhythm is originated in the SPZ-PVN region and transmitted to the SCN. A single ultradian bout is composed of multiple calcium transients that determine the amplitude of an ultradian bout by changing the frequency of transient. Ultradian bouts are synchronous throughout the SCN-SPZ-PVN regions, in which the TTX-sensitive neural network is involved. The NBQX- and APV-sensitive neurons could be the origin of ultradian oscillation. The gabazine-sensitive network is likely involved in the refinement of circadian output signals from the SCN. All experiments in this study were carried out on the SCN-SPZ-PVN culture slices from neonatal mice. Given that circadian properties of the cultured SCN slices develop in vitro similar to in vivo (39), the equivalent developmental stage in our long cultured slices is estimated around adolescence age (>P21). It waits for elucidation whether the adult mice show similar ultradian calcium rhythms in the SCN-SPZ-PVN region.

Materials and Methods

Animal Care. C57BL/6J mice (Clea Japan) were used for the experiments. Mice were born and bred in our animal quarters under controlled environmental conditions (temperature: 22 ± 2 °C, humidity: 60 ± 5%, 12-h light/12-h dark, with lights on from 0600 to 1800 hours). Light intensity was around 100 lx at the cage surface. The mice were fed commercial chow and tap water ad libitum. Experiments were conducted in compliance with the rules and regulations established by the Animal Care and Use Committee of Hokkaido University under the ethical permission of the Animal Research Committee of Hokkaido University (approval no. 15-0153).

SCN Slice Culture. The brains of neonatal mice (4- to 6-d-old both male and female) were obtained in the middle of the light phase under hypothermic anesthesia, and rapidly dipped in ice-cold balanced salt solution comprising 87 mM NaCl, 2.5 mM KCl, 7 mM MgCl$_2$, 0.5 mM CaCl$_2$, 1.25 mM NaH$_2$PO$_4$, 25 mM NaHCO$_3$, 25 mM glucose, 10 mM Hepes, and 75 mM sucrose. A 200-μm coronal slice containing the midstrocaudal region of the SCN and SPZ-PVN was carefully prepared using a vibratome (VT 1200; Leica), and explanted onto a culture membrane (Millicell CM; pore size, 0.4 μm; Millipore) in a 35-mm Petri dish containing 1 mL of DMEM (Invitrogen) and 5% FBS (Sigma-Aldrich). Before the recordings, the cultured slices were transferred to glass base dishes (35 mm, 3911-035; IWAKI). The dishes were sealed

with O$_2$-permeable filters (membrane kit, High Sens; YSI) using silicone grease compounds (SH111; Dow Corning Toray).

AAV-Mediated Gene Transfer into SCN Slices. An aliquot of the AAV (1 μL) harboring hSyn1-GCaMP6s (produced by the University of Pennsylvania Gene Therapy Program Vector Core) was inoculated onto the surface of the SCN culture at the seventh day of culture (*SI Appendix*, Fig. S1). The infected slice was further cultured for at least 10 d before imaging. The titer of hSyn1-GCaMP6s was 1.89 × 10^{13} genome copies per milliliter.

Imaging of Intracellular Calcium. Time-lapse wide-field imaging was conducted with an exposure time of 1–2 s (0.1–1 fps) at 10-min intervals (*SI Appendix*, Fig. S1B). Fast confocal imaging was conducted at 30 fps for 20 s and repeated this acquisition session at 10-min intervals over 2 d. The imaging system is composed of an EM-CCD camera (1,024 × 1,024 pixels, iXon3; Andor Technology), inverted microscope (Ti-E; Nikon), dry objectives (20 X, 0.75 NA, Plan Apo VC; Nikon), spinning-disk confocal system (X-Light; CREST OPTICS), box incubator (TIXHB; Tokai-hit), and MetaMorph software (Molecular Devices). The signal intensity at pixel level was far less than saturation level because the images were acquired at 16-bit data depth (0-65535), whereas the signal intensity in pixels in all slices was below 5,000. We confirmed in our previous study that lights of bright pixels in CCD camera did not affect the signals beyond a few neighboring pixels under similar experimental conditions to those of the present SCN-SPZ-PVN slices (25). GCaMP6s was excited by cyan color (475/28 nm) with the LED light source (Spectra X Light Engine; Lumencor) and the fluorescence was visualized with 495-nm dichroic mirror and 550/49-nm emission filters (Semlock). All experiments were performed at 36.5 °C and 5% CO$_2$. Tissue and cell condition were monitored by the bright field images of cultured slices and by the calcium signals in individual neurons. If we detected noticeable tissue damage during the recording, such as tissue swelling and abrupt/large calcium increase, which was usually followed by the permanent disappearance of fluorescence signals (this is the sign of cell death), we excluded the data for the analysis.

Mapping Circadian Parameters. For quantification of the circadian rhythms in the SCN, we used a custom-made program for the creation of acrophase maps as described previously (21, 23, 25, 46). The time series of the images in each pixel, {Yj (ti); ti = 1,2,...,N (h)}, was fitted to a cosine curve yj(t) = yj (t; Mj, Aj, Cj, Tj) = Mj + Aj × cosine (2pi (t − Cj)/Tj) using a least-square regression method, where j, yj (t) is the signal intensity at time t (h), Mj is the mesor, Aj is the amplitude, Cj is the acrophase, and Tj is the period of the images. Cosine curve fitting was applied in a period range between 18 and 30 h, and the goodness-of-fitting was statistically evaluated by Percent Rhythm, which accounted for the fitted cosine wave (Pearson product-moment correlation analysis) at a significance level of $P < 0.001$. The mean acrophase of the entire SCN regions was normalized to zero.

Data Analysis and Statistics. In all figures, the group data were presented as the mean ± SEM. Statistical analyses were performed using Excel (Microsoft) and Prism GraphPad (GraphPad Software). Paired or unpaired t tests were used when two dependent and independent group means were compared, respectively. One-way ANOVA with a post hoc Tukey–Kramer test was used to validate the drug effects when paired multiple group data were compared. Wavelet analysis was applied to evaluate ultradian and circadian rhythms in a range from 0 to 30 h, using MATLAB software and wavelet toolbox (MathWorks), with the bandwidth parameter setting to 3 and the center frequency to 1 (2). Ultradian calcium rhythms were expressed in a plotting along the x axis (2.4 h) and y axis (day) using ClockLab software (Actimetrics). The significance of the ultradian rhythm was evaluated by a χ^2 periodogram using ClockLab. A χ^2 periodogram was applied for a record of 48 h in a range between 2.2 and 3.8 h, with a significance level of $P < 0.01$.

To validate the circadian rhythmicity in the SPZ-PVN region, the fluorescence signals of 72 h recording in the ROIs in the whole SPZ-PVN region were fitted to a cosine curve using a least-squares regression method. The rhythmicity was evaluated by the goodness-of-fit (Percent Rhythm, $P < 0.001$) and amplitude (>mean + 3 SDs of the baseline intensity). For regional comparison of the rhythms in the SCN, ROIs (100 μm × 100 μm) in the upper one-third (near the third ventricle) and the lower one-third (near optic chiasma) were selected as the dorsal and ventral regions.

To measure the number and amplitude of ultradian bouts in the SPZ-PVN region, the highest and lowest calcium signals of the bout were normalized to 0–100% (Fig. 2C), and the mean values were obtained in the 72-h record. The circadian phases of the fitted curve were determined by four time windows: the peak, trough, falling, and rising phases (Fig. 2C). The falling and rising phases are defined as the phase between the 2 h before and 2 h

after the time point where the fitted signals on the rising and falling limbs cross a 50% level of the circadian amplitude, respectively (as shown by blue and red bands in Fig. 2C). The number of ultradian bouts was counted in the SPZ-PVN regions when the calcium signals exceed the threshold level which was the baseline by 5 SD of the signals determined in the presence of NBQX and APV ($n = 5$ slices). The acrophase was obtained from the cosine curve best fitted to successive calcium signals for 72 h in the SPZ-PVN and SCN region, separately (Fig. 2E).

The frequency of the fast calcium transients was analyzed by counting the number of transients per 20 s. In some ultradian bouts, the number of the transient was too large and the calcium signals became almost flat at a high level, which made correct counting difficult. In such a case, the time point was excluded for further analysis. The correlation between the amplitude of ultradian bout and the number of calcium transients were analyzed using all data points during the recording and assessed by a linear regression line.

Kinetics of calcium transients (frequency, rising time, amplitude, and one-half decay time) were calculated when the ultradian bout was below the threshold level (5 SD of the baseline signals). Twenty calcium transients in each slice were selected at random during 48-h recording and statistically compared among groups treated with different drugs by one-way ANOVA with a post hoc Tukey–Kramer test (*SI Appendix*, Fig. S13).

1. Reppert SM, Weaver DR (2002) Coordination of circadian timing in mammals. *Nature* 418:935–941.
2. Ono D, Honma K, Honma S (2015) Circadian and ultradian rhythms of clock gene expression in the suprachiasmatic nucleus of freely moving mice. *Sci Rep* 5:12310.
3. van der Veen DR, Gerkema MP (2017) Unmasking ultradian rhythms in gene expression. *FASEB J* 31:743–750.
4. Honma KI, Hiroshige T (1978) Endogenous ultradian rhythms in rats exposed to prolonged continuous light. *Am J Physiol* 235:R250–R256.
5. Dowse H, Umemori J, Koide T (2010) Ultradian components in the locomotor activity rhythms of the genetically normal mouse, *Mus musculus*. *J Exp Biol* 213:1788–1795.
6. Ueli S (2008) The mammalian circadian timing system. *Ultradian Rhythms from Molecules to Mind: A New Vision of Life*, ed David Lloyd ER (Springer, Berlin), pp 261–282.
7. Welsh DK, Takahashi JS, Kay SA (2010) Suprachiasmatic nucleus: Cell autonomy and network properties. *Annu Rev Physiol* 72:551–577.
8. Stephan FK, Zucker I (1972) Circadian rhythms in drinking behavior and locomotor activity of rats are eliminated by hypothalamic lesions. *Proc Natl Acad Sci USA* 69:1583–1586.
9. Eastman CI, Mistlberger RE, Rechtschaffen A (1984) Suprachiasmatic nuclei lesions eliminate circadian temperature and sleep rhythms in the rat. *Physiol Behav* 32:357–368.
10. Vitaterna MH, et al. (1994) Mutagenesis and mapping of a mouse gene, clock, essential for circadian behavior. *Science* 264:719–725.
11. Zheng B, et al. (1999) The mPer2 gene encodes a functional component of the mammalian circadian clock. *Nature* 400:169–173.
12. Choe HK, et al. (2013) Synchronous activation of gonadotropin-releasing hormone gene transcription and secretion by pulsatile kisspeptin stimulation. *Proc Natl Acad Sci USA* 110:5677–5682.
13. Nakamura W, et al. (2008) In vivo monitoring of circadian timing in freely moving mice. *Curr Biol* 18:381–385.
14. Kalsbeek A, Buijs RM (2002) Output pathways of the mammalian suprachiasmatic nucleus: Coding circadian time by transmitter selection and specific targeting. *Cell Tissue Res* 309:109–118.
15. Dibner C, Schibler U, Albrecht U (2010) The mammalian circadian timing system: Organization and coordination of central and peripheral clocks. *Annu Rev Physiol* 72:517–549.
16. Tousson E, Meissl H (2004) Suprachiasmatic nuclei grafts restore the circadian rhythm in the paraventricular nucleus of the hypothalamus. *J Neurosci* 24:2983–2988.
17. Hermes ML, Coderre EM, Buijs RM, Renaud LP (1996) GABA and glutamate mediate rapid neurotransmission from suprachiasmatic nucleus to hypothalamic paraventricular nucleus in rat. *J Physiol* 496:749–757.
18. Wang D, Cui LN, Renaud LP (2003) Pre- and postsynaptic GABA(B) receptors modulate rapid neurotransmission from suprachiasmatic nucleus to parvocellular hypothalamic paraventricular nucleus neurons. *Neuroscience* 118:49–58.
19. Lu J, et al. (2001) Contrasting effects of ibotenate lesions of the paraventricular nucleus and subparaventricular zone on sleep-wake cycle and temperature regulation. *J Neurosci* 21:4864–4874.
20. Enoki R, Ono D, Hasan MT, Honma S, Honma K (2012) Single-cell resolution fluorescence imaging of circadian rhythms detected with a Nipkow spinning disk confocal system. *J Neurosci Methods* 207:72–79.
21. Enoki R, et al. (2012) Topological specificity and hierarchical network of the circadian calcium rhythm in the suprachiasmatic nucleus. *Proc Natl Acad Sci USA* 109:21498–21503.
22. Chen T-W, et al. (2013) Ultrasensitive fluorescent proteins for imaging neuronal activity. *Nature* 499:295–300.
23. Enoki R, et al. (2017) Synchronous circadian voltage rhythms with asynchronous calcium rhythms in the suprachiasmatic nucleus. *Proc Natl Acad Sci USA* 114:E2476–E2485.
24. Enoki R, Ono D, Kuroda S, Honma S, Honma KI (2017) Dual origins of the intracellular circadian calcium rhythm in the suprachiasmatic nucleus. *Sci Rep* 7:41733.
25. Yoshikawa T, et al. (2015) Spatiotemporal profiles of arginine vasopressin transcription in cultured suprachiasmatic nucleus. *Eur J Neurosci* 42:2678–2689.
26. Li YF, Jackson KL, Stern JE, Rabeler B, Patel KP (2006) Interaction between glutamate and GABA systems in the integration of sympathetic outflow by the paraventricular nucleus of the hypothalamus. *Am J Physiol Heart Circ Physiol* 291:H2847–H2856.
27. Boudaba C, Tasker JG (2006) Intranuclear coupling of hypothalamic magnocellular nuclei by glutamate synaptic circuits. *Am J Physiol Regul Integr Comp Physiol* 291:R102–R111.
28. Israel J-M, Poulain DA, Oliet SHR (2010) Glutamatergic inputs contribute to phasic activity in vasopressin neurons. *J Neurosci* 30:1221–1232.
29. Israel JM, Le Masson G, Theodosis DT, Poulain DA (2003) Glutamatergic input governs periodicity and synchronization of bursting activity in oxytocin neurons in hypothalamic organotypic cultures. *Eur J Neurosci* 17:2619–2629.
30. Buijs RM, Kalsbeek A (2001) Hypothalamic integration of central and peripheral clocks. *Nat Rev Neurosci* 2:521–526.
31. Buijs RM, van Eden CG, Goncharuk VD, Kalsbeek A (2003) The biological clock tunes the organs of the body: Timing by hormones and the autonomic nervous system. *J Endocrinol* 177:17–26.
32. Walker JJ, Terry JR, Lightman SL (2010) Origin of ultradian pulsatility in the hypothalamic-pituitary-adrenal axis. *Proc Biol Sci* 277:1627–1633.
33. Swanson LW, Sawchenko PE (1980) Paraventricular nucleus: A site for the integration of neuroendocrine and autonomic mechanisms. *Neuroendocrinology* 31:410–417.
34. Honma S, Honma K (1985) Interaction between the circadian and ultradian rhythms of spontaneous locomotor activity in rats during the early developmental period. *Ultradian Rhythms in Physiology and Behavior*, eds Schulz H, Lavie P (Springer, Berlin), pp 95–109.
35. Meyer C, Freund-Mercier MJ, Guerné Y, Richard P (1987) Relationship between oxytocin release and amplitude of oxytocin cell neurosecretory bursts during suckling in the rat. *J Endocrinol* 114:263–270.
36. Aschoff J (1965) Response curves in circadian periodicity. *Circadian Clocks*, ed Aschoff J (North-Holland, Amsterdam), pp 95–111.
37. Abe M, et al. (2002) Circadian rhythms in isolated brain regions. *J Neurosci* 22:350–356.
38. Yamaguchi S, et al. (2003) Synchronization of cellular clocks in the suprachiasmatic nucleus. *Science* 302:1408–1412.
39. Ono D, Honma S, Honma K (2013) Cryptochromes are critical for the development of coherent circadian rhythms in the mouse suprachiasmatic nucleus. *Nat Commun* 4:1666.
40. Rusakov DA, Fine A (2003) Extracellular Ca2+ depletion contributes to fast activity-dependent modulation of synaptic transmission in the brain. *Neuron* 37:287–297.
41. Bikson M, et al. (2004) Effects of uniform extracellular DC electric fields on excitability in rat hippocampal slices in vitro. *J Physiol* 557:175–190.
42. Hirata H, et al. (2002) Oscillatory expression of the BHLH factor Hes1 regulated by a negative feedback loop. *Science* 298:840–843.
43. Shimojo H, Kageyama R (2016) Oscillatory control of Delta-like1 in somitogenesis and neurogenesis: A unified model for different oscillatory dynamics. *Semin Cell Dev Biol* 49:76–82.
44. Lewandowski MH, Błasiak T (2004) Slow oscillation circuit of the intergeniculate leaflet. *Acta Neurobiol Exp (Warsz)* 64:277–288.
45. van den Pol AN, Finkbeiner SM, Cornell-Bell AH (1992) Calcium excitability and oscillations in suprachiasmatic nucleus neurons and glia in vitro. *J Neurosci* 12:2648–2664.
46. Honma S, et al. (2016) Oscillator networks in the suprachiasmatic nucleus: Analysis of circadian parameters using time-laps images. *Biological Clocks–30th Anniversary of Sapporo Symposium on Biological Rhythm*, eds Honma K, Honma S (Hokkaido Univ Press, Sapporo, Japan), pp 33–41.